

Integrated quantum polariton interferometry

Davide Nigro^{1✉}, Vincenzo D'Ambrosio², Daniele Sanvitto³ & Dario Gerace^{1✉}

Exciton-polaritons are hybrid radiation-matter elementary excitations that, thanks to their strong nonlinearities, enable a plethora of physical phenomena ranging from room temperature condensation to superfluidity. While polaritons are usually exploited in a high-density regime, evidence for quantum correlations at the level of few excitations has been recently reported, thus suggesting the possibility of using these systems for quantum information purposes. Here we show that integrated circuits of propagating single polaritons can be arranged to build deterministic quantum logic gates in which the two-particle interaction energy plays a crucial role. Besides showing their prospective potential for photonic quantum computation, we also show that these systems can be exploited for metrology purposes, as for instance to precisely measure the magnitude of the polariton-polariton interaction at the two-body level. Our results will motivate the development of practical quantum polaritonic devices in prospective quantum technologies.

¹Dipartimento di Fisica, Università di Pavia, via Bassi 6, I-27100 Pavia, Italy. ²Dipartimento di Fisica, Università di Napoli Federico II, Complesso Universitario di Monte Sant'Angelo, Via Cintia, 80126 Napoli, Italy. ³CNR NANOTEC, Institute of Nanotechnology, Campus Ecotekne, Via Monteroni, 73100 Lecce, Italy. ✉email: dadde.nigro@gmail.com; dario.gerace@unipv.it

Exciton-polaritons have been emerging as a promising platform to explore fundamental physics effects in an analog solid state scenario, such as Bose-Einstein condensation^{1,2}, superfluidity³, soliton propagation⁴, spontaneous formation of vortices⁵, Josephson oscillations and self-trapping⁶, analog gravity⁷. In parallel, their nonlinear properties have been exploited to deliver more application-oriented devices, such as all-optical transistors⁸, resonant tunnel diodes⁹, Mach-Zehnder interferometers¹⁰, routers¹¹, couplers¹², or ultra-low-threshold lasers¹³, just to mention a few. In addition, polariton integrated circuits have been proposed in view of mimicking the key functionalities of electronic circuits¹⁴, or to implement artificial neural networks¹⁵.

All these fascinating results and perspectives are a consequence of the microscopic nature of polariton excitations, which are characterized by a coherent superposition of two very different fields, the electromagnetic (photon) field and an optically active polarization (the exciton), i.e., a collective crystal excitation made of a bound electron-hole pair¹⁶. As such, the polariton field inherits the small effective mass ($\sim 10^{-5}$ relative to the free electron mass) of bound photonic modes, e.g., in a planar microcavity or waveguide^{17,18}. In addition, it also inherits the large nonlinearity (comparatively, estimated to be about 4 orders of magnitude larger than bulk silicon) derived from the Coulomb interaction between excitons^{19,20}.

At high excitation density (but well below the saturation regime), the polariton mean field is described in terms of a non-equilibrium Gross-Pitaevskii equation, which has been successfully applied to interpret most of the quantum fluid phenomenology observed, so far²¹. In this regime, confined polaritons can be effectively treated as an out-of-equilibrium gas of weakly interacting bosons, whose steady state depends on the balance between driving and losses in the system. Recently, exciton-polariton condensates have also been proposed for quantum information processing, with the proposal of encoding qubits into the quantum fluctuations on top of the condensate²², or in the polariton spin degrees of freedom²³.

In the last few years experiments have shown the possibility to excite the quantized polariton field in confined geometries at the level of single or few excitation quanta^{24,25}, and evidence of quantum correlations at the level of few polariton excitations has been reported^{26,27}. In such a regime, however, the mean field treatment does not provide an accurate theoretical description, calling for a more appropriate open quantum system approach to describe strongly interacting polaritons²¹. Hence, triggered by all these promising experimental results, as well as by the thrilling perspective to perform quantum computational tasks by means of polariton-based devices, we have been motivated to provide an in-depth theoretical analysis of integrated polariton circuits in the quantum regime, with particular attention to the differences with respect to linear photonic integrated circuits and to the unique possibilities enabled by nonlinearities introduced by polariton interactions. In our view, such *quantum polariton integrated circuits* (QPIC) can be assumed as complex networks resulting from the combination of n coupled *nonlinear* waveguides and interferometers, in which polaritons can be injected and propagate while interacting at the level of few quanta.

It is worth stressing, however, that the precise characterization of a device having an arbitrary large number n of propagation channels with $m < n$ single-photon inputs, even in the *linear* regime and by means of advanced numerical tools, is already a challenging task to be solved. In fact, this problem has recently attracted a great deal of attention, both in theory and experiments, aiming at exploiting quantum resources to demonstrate the solution of a problem that no classical computer can solve in a feasible amount of time, the so called quantum supremacy^{28–31}. It

has been conjectured that the presence of nonlinearities may be beneficial to reach quantum supremacy in this context³². More in general, nonlinearities can be a crucial resource in the quest for the development of photonic quantum gates. Indeed, while original proposals only employing linear optical elements lead to a non-deterministic computing scenario^{33,34}, novel ideas aimed at developing deterministic quantum gates based on effective photonic interactions have been put forward^{35–37}. Realizing deterministic quantum photonic gates would represent a significant milestone for quantum technologies in near-term devices³⁸. In light of these developments, the intrinsically large polariton nonlinearity may thus play a key role.

In this respect, we remind that there has been a longstanding debate to quantitatively measure the polariton-polariton nonlinearity³⁹, and only recently the corresponding order of magnitude has been more precisely inferred from photon-photon correlation measurements²⁷. An increase in the magnitude of this parameter, induced by a strong electric field, has also been reported^{40,41}. On the other hand, no quantitatively accurate measure of this parameter exists, to date. This is because most of these measurements are performed in the regime of large polariton density, typically treated at the mean field level, and whose nonlinear behavior is fully characterized by the product of inter-particle interaction energy and particle density. In practice, disentangling these two contributions is at the origin of large uncertainties in the determination of the inter-particle contribution alone.

Here we focus our theoretical description on a realistic experimental configuration in which single photons are coupled onto a semiconductor device in which polariton excitations exist and can be guided on chip⁴². In such a situation, single photons are converted into single polariton wave packets that retain the quantum radiation field coherence properties^{24,25}, and can then be interfered through evanescently coupled waveguides alternated with regions of free propagation, as illustrated in Fig. 1. We show that it is possible to realize nonlinear quantum devices by exploiting polariton-polariton interactions that are naturally present in a QPIC. In particular, we introduce a scheme to implement a deterministic two-qubits quantum gate, specifically the $\sqrt{\text{SWAP}}$ gate introduced in ref. 43 and defined in Eq. (27). Such a gate can be used in combination with single qubit operations to implement the CNOT gate (thus, *any* quantum gate⁴⁴). Therefore our results demonstrate that QPICs represent a promising platform for the development of integrated photonic devices for universal quantum computing, going beyond currently accepted non-deterministic paradigms based on linear optical elements. The functionalities introduced by QPICs can

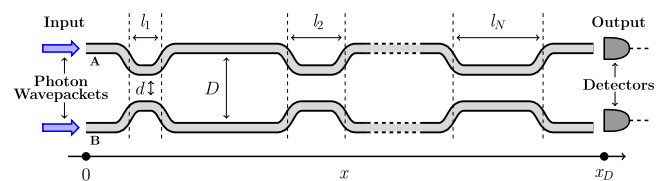


Fig. 1 Generic QPIC with two input and output channels. It is assumed that pairs of polaritons are created at $x = 0$ and many-body interactions are then detected at x_D by measuring the degree of correlation of photons emerging from the two channels. In this work, we will assume that each input is a single photon state. The device consists of a sequence of N interaction regions of length l_j ($j = 1, 2, \dots, N$) where the two waveguides (labeled as A and B) run in parallel at a distance equal to d so that they are evanescently coupled. Two consecutive interaction regions are separated by a free-propagation region, that is a portion of the device where the distance between the two waveguides is $D \gg d$ and the coupling between the two waveguides is negligible.

then be exploited in addition to (or in combination with) the usual linear optical interferometers employed in conventional photonic circuits (PCs)^{45–47}. In addition, the QPICs are shown to hold promise also in quantum metrology. In particular, we show how they potentially allow to measure with high precision the two-polariton nonlinear shift by exploiting Fock states interference. More generally speaking, while the framework here developed may pave the way for the realization of quantum technologies specifically enabled by large polariton interactions, it should be noticed that the same theoretical analysis fully applies to any potential quantum photonic platform possessing significant third-order nonlinearity. In this respect, applications of QPIC ranging from quantum metrology, simulations, and sensing, to quantum information processing and computing, may ultimately be envisaged.

Results

Model and theory. We start by briefly outlining the theoretical model that will be exploited to describe polariton-polariton interactions at the two-particle level in QPICs. In what follows, we will only consider the Hamiltonian unitary evolution, which already allows to grasp the effects of two-particle interactions on quantum correlations. In fact, long lived polaritonic excitations⁴⁸, and propagation lengths in the order of 400 μm ²⁵, justify our unitary approach if restricted to devices with limited length. However, a quantitative description of the effects of particle losses, unavoidably present in realistic experimental situations, is given in Supplementary information (SI), see Supplementary Note 3, showing how such incoherent processes do not affect the output photon statistics derived in the unitary case.

Modeling the time evolution. The effective Hamiltonian model used to describe the propagation of polaritons in the two co-directional waveguides sketched in Fig. 1 reads ($\hbar = 1$)

$$\hat{\mathcal{H}} = \sum_k \left[\hat{\mathcal{H}}_k^a + \hat{\mathcal{H}}_k^b + J(x) \left(\hat{a}_k^\dagger \hat{b}_k + \hat{b}_k^\dagger \hat{a}_k \right) \right], \quad (1)$$

in which $\hat{a}_k^{(\dagger)}$ and $\hat{b}_k^{(\dagger)}$ denote the annihilation (creation) operators of a polariton with wavevector k in the waveguide A and B respectively, and $\hat{\mathcal{H}}_k^\sigma = \omega_k \hat{\sigma}_k^\dagger \hat{\sigma}_k + U_k \hat{\sigma}_k^\dagger \hat{\sigma}_k^\dagger \hat{\sigma}_k \hat{\sigma}_k$ ($\sigma = a, b$) represents the Hamiltonian of each waveguide in the lower polariton branch. A detailed derivation of this model from the coupled exciton-photon fields is reported in Supplementary Note 1. In particular, the interaction energy U_k accounts for the two-body interaction arising from the exciton fraction in polaritons at given wave vector k . The last term in Eq. (1) describes hopping between the two waveguides, which is due to the evanescent coupling between the photonic fractions of the co-propagating polaritons in A and B channels, respectively. This is formally equivalent to a beam splitter Hamiltonian in quantum optics. We can generically assume that the tunnel coupling energy, $J(x)$, is a space-dependent parameter only determined by the physical distance between the two channels at position x along the propagation direction. Furthermore, since the evanescent fields in each waveguide decay exponentially, hopping is expected to be suppressed when increasing the separation between the two channels, while being effectively present only in the regions where the two waveguides are close enough. As a consequence, it is reasonable to assume $J(x)$ to be non-zero and equal to a constant value, $J > 0$, only when the distance is d , and zero elsewhere.

In our scenario, we envision single-polariton quanta to be created in the integrated device by shining single photons on the leftmost side of the device, at $x = 0$, and their properties (for instance, polariton-polariton correlations) are subsequently measured by detecting photons emerging on the rightmost side

of the apparatus, at $x = x_D$. In particular, we consider the initial state as a product state, that is

$$|\psi(t = 0)\rangle = |\psi_A(t = 0)\rangle \otimes |\psi_B(t = 0)\rangle, \quad (2)$$

with $|\psi_A(t = 0)\rangle$ and $|\psi_B(t = 0)\rangle$ describing the initial state of the waveguide A and B respectively. While at $t = 0$ the quantum system is in a product state, at $t > 0$ it will be in a superposition of different quantum states. In addition to the obvious dependence on geometrical aspects, such as the length of the interaction regions ($\{l_j\}$) and the separation between the waveguides, the degree of correlation present in $|\psi(t)\rangle$ does depend on several factors, ranging from the number of initial photons injected into the system, to their temporal and spatial shape. In the present paper we will only consider the cases where the initial state corresponds to either (i) a single polariton, or (ii) a product of two single-polariton Fock states. Furthermore, we assume in both cases to have particles with the same wavevector, k . More explicitly, in what follows we consider single polariton states as

$$|\psi(t = 0)\rangle = \hat{a}_k^\dagger |\Omega\rangle \equiv |1_k^A, 0_k^B\rangle, \quad (3)$$

or

$$|\psi(t = 0)\rangle = \hat{b}_k^\dagger |\Omega\rangle \equiv |0_k^A, 1_k^B\rangle, \quad (4)$$

and two-polariton states as

$$|\psi(t = 0)\rangle = \hat{a}_k^\dagger \hat{b}_k^\dagger |\Omega\rangle \equiv |1_k^A, 1_k^B\rangle, \quad (5)$$

with $|\Omega\rangle$ denoting the polariton vacuum in each propagating channel.

Before going any further in our theoretical discussion, it is worth stressing that it is nowadays possible to engineer photon sources having the desired properties needed for the creation of the few polaritons states assumed as the inputs of the devices characterized in the following. Indeed, it has been experimentally shown that single quantum emitters can be used as bright sources of single-photon Fock states, with very high photon-number purity, and near-unity indistinguishability^{49,50}. Therefore, we consider a realistic experimental setup exploiting single quantum emitters as input stages (similarly to what has already been shown²⁵) whose single photons are used to feed the QPICs described in the following sections, therefore initializing the interferometer with the polariton states defined in Eqs. (3), (4) and (5), respectively.

Single-polariton dynamics. The single polariton states in Eqs. (3) and (4) are not affected by interaction terms proportional to U_k , and their evolution through the QPIC in Fig. 1 is only sensitive to the regions where $J(x) \neq 0$. Let us assume now that a polariton state with wavevector k corresponds to a particle propagating at a constant speed given by its group velocity, that is

$$v_g = \frac{\partial \omega_k}{\partial k}, \quad (6)$$

with ω_k being the single-polariton dispersion entering in the Hamiltonian model. This implies that, in order to propagate across the m -th interaction region of length l_m , the quantum particle needs roughly a time given by

$$t_m = \frac{l_m}{v_g}. \quad (7)$$

In addition, by observing that such states are in one-to-one correspondence with the two polarization states of a spin-1/2 particle, that is

$$|\uparrow\rangle = |1_k^A, 0_k^B\rangle, \quad |\downarrow\rangle = |0_k^A, 1_k^B\rangle, \quad (8)$$

their evolution through an interaction length $l = v_g t$ is prescribed

by the following unitary operator

$$U_{IR}^{(1)}(t) = e^{-i\hat{H}t} = e^{-i\omega_k t} (\cos(Jt)\mathbb{1} - i \sin(Jt)\sigma_x), \tag{9}$$

with $\hat{H} = \omega_k\mathbb{1} + J\sigma_x$, with $\mathbb{1}$ and σ_x being the identity and the Pauli-X matrices respectively. The subscript IR stands for “Interaction region”.

In particular, notice that in correspondence of the following values of the propagation time ($\hbar = 1$)

$$T_{dip}^{(n)} = \frac{\pi}{4J} (1 + 2n), \tag{10}$$

with n being any integer, the operator in Eq. (9) describes a 50:50 beamsplitter. In practice, this means that if one properly chooses the interaction length l and the group-velocity v_g in such a way that the ratio l/v_g equals $T_{dip}^{(n)}$ for some integer n , then any initial single-polariton state, such as one of Eqs. (3) and (4), is mapped into an equally weighted superposition of the two. For instance, in correspondence of $T_{dip}^{(0)} \equiv T_{dip}$, one has that

$$U_{IR}^{(1)}(T_{dip})|1_k^A, 0_k^B\rangle = \frac{|1_k^A, 0_k^B\rangle - i|0_k^A, 1_k^B\rangle}{\sqrt{2}} \tag{11}$$

and

$$U_{IR}^{(1)}(T_{dip})|0_k^A, 1_k^B\rangle = \frac{|0_k^A, 1_k^B\rangle - i|1_k^A, 0_k^B\rangle}{\sqrt{2}}. \tag{12}$$

In the next section we discuss the propagation of the two-polariton state in Eq. (5) through a generic QPIC. We show that it is possible to map the polariton-polariton dynamics into that of a two-level atom driven by external electromagnetic pulses.

Dynamics of two identical polaritons. Starting from a double excitation subspace (i.e., an initial configuration with a total number of two polaritons in the system), the quantum state evolves in time as the following superposition

$$|\psi(t)\rangle = \alpha(t)|1_k^A, 1_k^B\rangle + \beta(t)|2_k^A, 0_k^B\rangle + \gamma(t)|0_k^A, 2_k^B\rangle, \tag{13}$$

where we introduced the states $|2_k^A, 0_k^B\rangle = (\hat{a}_k^\dagger)^2|\Omega\rangle/\sqrt{2}$ and $|0_k^A, 2_k^B\rangle = (\hat{b}_k^\dagger)^2|\Omega\rangle/\sqrt{2}$. Therefore, in the general case, the time evolution of any two-polariton input state can be effectively described by means of a three level system, and the coefficients $\alpha(t)$, $\beta(t)$, and $\gamma(t)$ are only related by the normalization condition on $|\psi\rangle$. However, by considering that the Hamiltonian is symmetric under the exchange of \hat{a}_k and \hat{b}_k , the input state in Eq. (5) evolves as:

$$|\psi(t)\rangle = \alpha(t)|1_k^A, 1_k^B\rangle + \beta(t)(|2_k^A, 0_k^B\rangle + |0_k^A, 2_k^B\rangle). \tag{14}$$

Therefore, by defining

$$|g\rangle = |1_k^A, 1_k^B\rangle, \quad |e\rangle = \frac{|2_k^A, 0_k^B\rangle + |0_k^A, 2_k^B\rangle}{\sqrt{2}}, \tag{15}$$

the Hamiltonian model in Eq. (1) can be expressed on this basis, reading

$$\hat{H} = (2\omega_k + U_k)\mathbb{1} + 2J(x)\sigma_x - U_k\sigma_z, \tag{16}$$

where $\mathbb{1}$, σ_x , and σ_z are the identity and the Pauli-X and Z matrices, respectively. In particular, in our representation $\sigma_z|g\rangle = |g\rangle$ and $\sigma_z|e\rangle = -|e\rangle$.

This model equivalently describes a two-level atom propagating in free space with transition frequency/detuning given by $2U_k$, and effectively interacting with a transverse field, \vec{F} , producing a Rabi frequency $2J(x)$, and $|g\rangle$ ($|e\rangle$) corresponds to the ground (excited) state of such fictitious atom. In other words, the

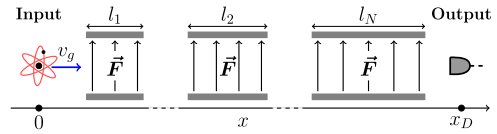


Fig. 2 Atom-polariton correspondence. Schematic picture of a physical system whose dynamical evolution is equivalent to that of the propagating two-polariton state defined in Eq. (5): A two-level atom is injected from the left with speed v_g (in analogy with the polariton group velocity) and propagates towards the detection region ($x = x_D$), through regions characterized by the presence or absence of an external transverse electric field, \vec{F} .

propagation of the state in Eq. (5) through the QPIC reported in Fig. 1, is equivalent to the physical situation pictured in Fig. 2. On the left (input side), there is an atom initially prepared in the $|g\rangle$ state. Such a particle is then sent at speed v_g through a sequence of regions having different properties, i.e. with or without the external transverse field \vec{F} , and its properties are read on the rightmost side of the apparatus (output region). In particular, we assume that in between the regions represented in Fig. 2 and characterized by a length l_j , there are regions where the atom can propagate freely, i.e. $\vec{F} = \vec{0}$. Similarly to what happens in the one particle sector, the faster the atom moves (i.e., the larger v_g), the smaller is the time spent by polaritons in each hopping regions, and thus the smaller is the probability of observing a polariton jumping from a waveguide to the adjacent one. On the other hand, in the two-particle subspace of the Hamiltonian (1), the terms depending on U_k play a non negligible role. In particular, following Eq. (16), and by virtue of the properties of the Pauli matrices, the propagation within the polariton interferometer depicted in Fig. 1 is completely determined by composing the proper number of times two unitary operators

$$U_{IR}^{(2)}(t) = e^{-i\phi t} \left[\cos\left(\sqrt{U_k^2 + 4J^2}t\right)\mathbb{1} + i \frac{\sin\left(\sqrt{U_k^2 + 4J^2}t\right)}{\sqrt{U_k^2 + 4J^2}} (-2J\sigma_x + U_k\sigma_z) \right], \tag{17}$$

and

$$U_{FP}^{(2)}(t) = e^{-i\phi t} [\cos(U_k t)\mathbb{1} + i \sin(U_k t)\sigma_z], \tag{18}$$

where $\phi = 2\omega_k + U_k$ and the subscript FP stands for “free propagation”. The operator in Eq. (17) describes the evolution of an initially symmetric state along an interaction length $l = v_g t$, while the one in Eq. (18) describes the evolution of the two-polariton system in the free propagation region between two interaction regions. In particular, notice that $U_{FP}^{(2)}(t)$ introduces a phase difference between the states $|g\rangle$ and $|e\rangle$, which is proportional to $2U_k$.

Applications. In this section we consider two paradigmatic cases of the generic QPIC, showing how these devices can be used for either precisely measuring the interaction strength between two single polaritons or implementing nonlinear quantum gates. A generalized version of the solution corresponding to the case of ideally lossless polariton propagation is reported in SI, see Supplementary Notes 2–3.

Single hopping region: nonlinear HOM effect. The most elementary building block of a QPIC, namely a single region of evanescent coupling between waveguides A and B, characterized by the length l , is depicted in Fig. 3. This configuration is typically exploited in

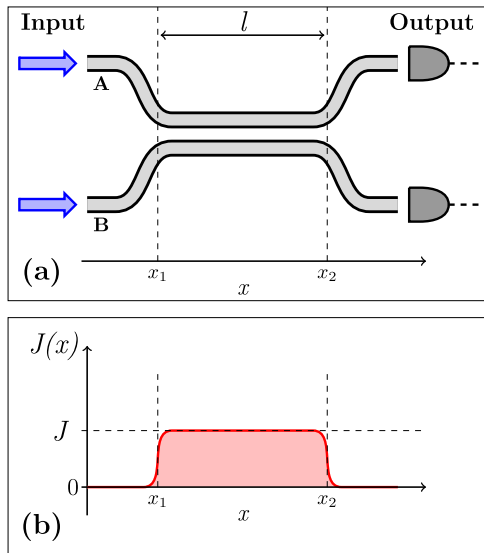


Fig. 3 Elementary QPIC with single hopping region. **a** Sketch of a polariton circuit made of a pair of co-propagating waveguides, labeled as A and B, which are coupled along a spatial region of length l . **b** Schematic behavior of the coupling constant, $J(x)$, describing the evanescent coupling between the two waveguides of the polariton circuit described in **a**. In this setup, the coupling is non-zero and equal to a constant value J only in the region $x_1 < x < x_2$.

conventional PCs to realize a beamsplitter. Here, the main difference is the presence of the polariton number-dependent nonlinear interaction within the single waveguide channel, which is going to alter the beam splitting condition, as well as influencing the many particle statistics in each channel. In order to characterize the quantum behavior of the device, we will consider the auto- and cross-correlation functions at the output ports, defined as

$$G_{AA}(t, U_k/J) = \langle \psi(t) | \hat{a}_k^\dagger \hat{a}_k^\dagger \hat{a}_k \hat{a}_k | \psi(t) \rangle, \quad (19)$$

and

$$G_{AB}(t, U_k/J) = \langle \psi(t) | \hat{a}_k^\dagger \hat{b}_k^\dagger \hat{b}_k \hat{a}_k | \psi(t) \rangle, \quad (20)$$

where t is the polariton arrival instant at the rightmost end of the device. Here, polaritons are converted into photons. Therefore, the former amplitude represents the probability of having two photons emerging in pairs from the waveguide A, and $G_{AA}(t, U_k/J) = G_{BB}(t, U_k/J)$ by symmetry. The other amplitude, $G_{AB}(t, U_k/J)$, accounts for events related to photons simultaneously emerging (and being detected) from different waveguides. Following Eq. (17), after some algebra, analytic expressions can be obtained, which read:

$$G_{AA}(t, U_k/J) = \frac{2J^2}{U_k^2 + 4J^2} \sin^2 \left(\sqrt{U_k^2 + 4J^2} t \right) \quad (21)$$

and

$$G_{AB}(t, U_k/J) = 1 - 2G_{AA}(t, U_k/J). \quad (22)$$

The dependence of G_{AA} and G_{AB} on U_k/J is shown in Fig. 4, where we plot the dependence of these correlation functions on the time spent by the two polariton wave packets in the region of length l . This time is compared to the parameter T_{dip} , which corresponds to the time for which the device would behave as a regular 50:50 beam splitter in the absence of polariton interactions, i.e. for $U_k/J = 0$. In fact, this can be interpreted as the time for which the interferometer results in the well known Hong-Ou-Mandel (HOM) effect in conventional PCs^{45,51–54}. Such an established phenomenon is related to the bosonic nature

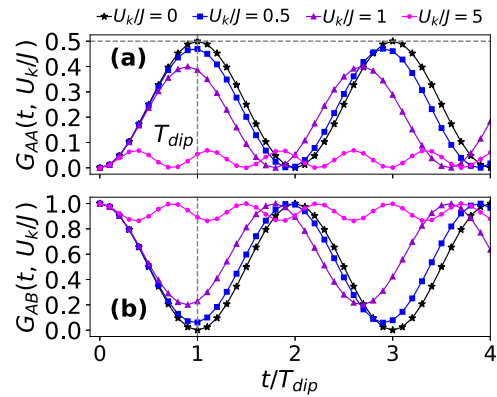


Fig. 4 Correlation functions of elementary QPIC. Behaviors of **a** the auto-correlation $G_{AA}(t, U_k/J)$ and **b** the cross-correlation $G_{AB}(t, U_k/J)$ as a function of the time spent within the hopping region of length l , and for different values of the ratio U_k/J . This time, t , is given in units of $T_{dip} = \pi/(4J)$. The vertical dashed lines at $t/T_{dip} = 1$ identify the occurrence of the Hong-Ou-Mandel effect for $U_k/J = 0$. At such condition (as well as for $t/T_{dip} = 2n + 1$, with n being an integer, see Eq. (10)), the linear QPIC behaves as a 50:50 beam-splitter. As a consequence, the auto- and cross-correlation functions are at maximum and minimum values, respectively, i.e., $G_{AA}(t = T_{dip}, U_k/J = 0) = 0.5$ and $G_{AB}(t = T_{dip}, U_k/J = 0) = 0$.

of two indistinguishable particles going through a 50:50 beam splitter from two different input ports, and it is characterized by a dip in the probability of simultaneously detecting the two particles emerging from different output ports, ideally going to zero, due to the destructive interference of their probability amplitudes⁵⁵. In our notation, this corresponds to the condition for which $G_{AB}(T_{dip}, 0) = 0$. At the same time, this condition also implies that the probability of observing two bosons emerging in pairs from the same waveguide is maximized (boson bunching), i.e. $G_{AA}(T_{dip}, 0) = G_{BB}(T_{dip}, 0) = 0.5$. This is shown in the plots of Fig. 4 for $U_k/J = 0$ and $t/T_{dip} = 1$, with an obvious periodicity as a function of t/T_{dip} . However, while the HOM effect has been mostly explored in linear interferometers, so far, our framework allows to straightforwardly address the effect of polariton nonlinearities. In particular, the HOM dip tends to be suppressed on increasing U_k/J , i.e. strong polariton correlations inhibit the quantum interference at the beam splitting condition. More in detail, as suggested by the results in Eqs. (21) and (22), for $U_k/J \gg 1$ (i.e., what we define the strongly correlated polariton regime) the probability of observing photons emerging in pairs from the same waveguide becomes negligible, while photons are mostly expected to be simultaneously detected from the two different output channels, i.e.

$$G_{AA}(t, U_k/J) \rightarrow 0, \quad G_{AB}(t, U_k/J) \rightarrow 1 \quad (23)$$

The detailed convergence to this regime as a function of the relevant scale U_k/J is explicitly shown in Fig. 5. Here we plot the behavior of the two amplitudes defined in Eqs. (21) and (22) for $t/T_{dip} = 1$, and the maximum and minimum value they respectively reach while varying the ratio t/T_{dip} , i.e. corresponding to an interaction time $\tilde{t} \equiv \pi/(2\sqrt{U_k^2 + 4J^2})$.

Essentially, this behavior can be interpreted as follows: on increasing the on-site interaction within each propagating channel, the bunching probability is suppressed. In quantum photonics, this is reminiscent of the polariton blockade effect^{56,57}, recently evidenced in confined geometries^{26,27}. Evidently, if such a regime could be accessed in a propagating geometry, the device would implement a kind of nonlinear beam splitter in which bosonic coalescence is destroyed in favor of “fermionization” induced by strong interactions^{58,59}.

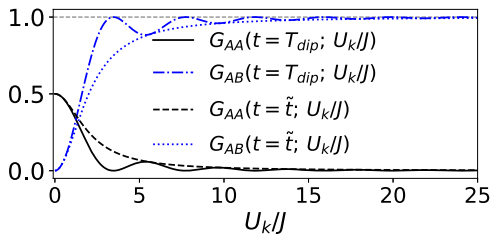


Fig. 5 Correlations dependence from polariton nonlinearity. The curves labeled as $G_{AA}(t = T_{dip}, U_k/J)$ and $G_{AB}(t = T_{dip}, U_k/J)$ describe the behavior of auto- and cross-correlation functions, respectively, for $t = T_{dip}$ and as a function of the polariton two-body interaction, U_k/J . The condition $U_k/J = 0$ corresponds to the Hong-Ou-Mandel effect, i.e., $G_{AA}(t = T_{dip}, U_k/J = 0) = 0.5$ and $G_{AB}(t = T_{dip}, U_k/J = 0) = 0$, respectively. Dotted and dashed curves describe the dependence of the G_{AA} maximum and G_{AB} minimum values, respectively, on U_k/J . Such a condition is identified by $t = \tilde{t}$, with $\tilde{t} = \pi/(2\sqrt{U_k^2 + 4J^2})$.

More practically, even being limited to the realm of weak nonlinearities that do not allow to access such strong correlation regime, this configuration may still allow to directly assess interaction-induced deviations from the HOM condition. However, as it will be detailed in the “Discussion” section, polariton interaction energies have been reported in the few μeV range, which are too small to be detected on the scale of the plot in Fig. 5 (J is typically in the meV order of magnitude, thus $U_k/J < 1$). The scheme in Fig. 3, on the other hand, is just the simplest building block for QPICs. Nevertheless, as discussed in the following section, by exploiting a slightly more complex scheme it is possible to design polariton circuits showing enhanced sensitivity to the critical parameter U_k/J . The latter could be exploited, in turn, to implement quantum gates for polaritons encoding information even in the presence of small nonlinearities, as pointed out in the following.

Two hopping regions: polariton Ramsey interferometer. Motivated by the nonlinear HOM results shown before, and by the atom-polariton correspondence previously discussed in the “Model and Theory” subsection, in relation to the “Dynamics of two identical polaritons”, here we explore the dynamics and the resulting quantum correlations at the output of the device depicted in Fig. 6. In this case, the hopping is split into two separate regions having the same length, l , and separated by a free propagation region within each waveguide. As previously done, we define the time spent in each interaction region, t , and the time spent in the region $x_2 < x < x_3$, T , as the relevant parameters. Given these definitions, the action of the device in Fig. 6 on the two polariton state defined in Eq. (5) is described by the unitary operator

$$U(t, T) \equiv U_{IR}^{(2)}(t)U_{FP}^{(2)}(T)U_{IR}^{(2)}(t). \quad (24)$$

In particular, a direct analytic computation shows that the probability of having two photons being detected from the same output channel after the second hopping region reads

$$G_{AA}(t, T; U_k/J) = \frac{2J^2}{(U_k^2 + 4J^2)} \sin^2(2\theta t) \cos^2(U_k T) - \frac{2J^2 U_k}{(U_k^2 + 4J^2)^{3/2}} \sin^2(\theta t) \sin(2\theta t) \sin(2U_k T) + \frac{8J^2 U_k^2}{(U_k^2 + 4J^2)^2} \sin^4(\theta t) \sin^2(U_k T), \quad (25)$$

with $\theta = \sqrt{U_k^2 + 4J^2}$. Similarly to the previous case, we have

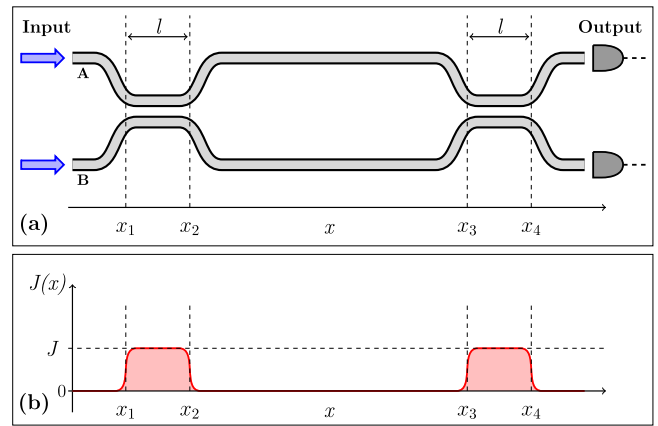


Fig. 6 Analog Ramsey interferometer in QPIC. **a** Sketch of a polariton circuit made of two identical hopping regions of length l separated by a free propagation region. **b** Sketch of the spatial dependence of the hopping parameter $J(x)$ along the device in **a**. As in the case of the elementary QPIC in Fig. 3, we consider $J(x) = J$ in the two interaction regions and zero elsewhere.

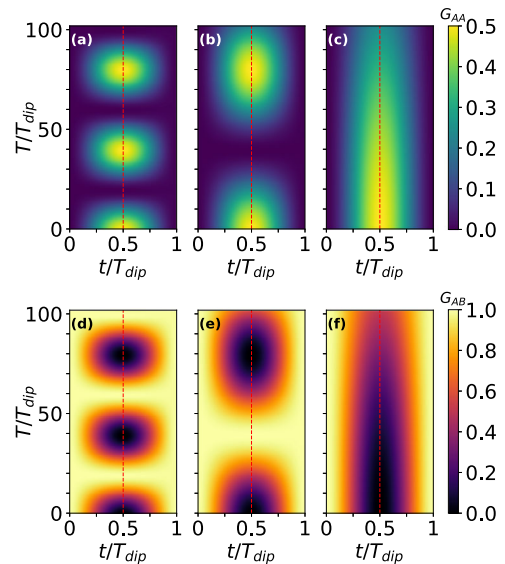


Fig. 7 Global correlations behavior in the analog Ramsey setup. Color scale plot showing the dependence of G_{AA} (Eq. (25)) on both t/T_{dip} and T/T_{dip} for **a** $U_k/J = 0.1$, **b** $U_k/J = 0.05$, and **c** $U_k/J = 0.01$. Similarly, we also report the color scale plot with the dependence of G_{AB} (Eq. (26)) on t/T_{dip} and T/T_{dip} , for **d** $U_k/J = 0.1$, **e** $U_k/J = 0.05$, and **f** $U_k/J = 0.01$. Vertical lines have been added to each panel as a guide to the eye in evidencing the condition $t/T_{dip} = 0.5$.

$G_{BB} = G_{AA}$ and

$$G_{AB}(t, T; U_k/J) = 1 - 2G_{AA}(t, T; U_k/J). \quad (26)$$

Here, it is worth highlighting the explicit dependence of the correlation functions on t , for which the degree of correlation of the output photons can be modulated by either changing the interaction length, l , or the separation between the two hopping regions, i.e., the time T .

Globally, the behavior of $G_{AA}(t, T; U_k/J)$ and $G_{AB}(t, T; U_k/J)$ for different values of U_k/J , and as a function of both t/T_{dip} and T/T_{dip} , is reported in Fig. 7. Correlation functions display a periodic dependence on T/T_{dip} . In particular, for all the values of U_k/J considered, the probability of having photons emerging simultaneously from the same waveguide, quantified

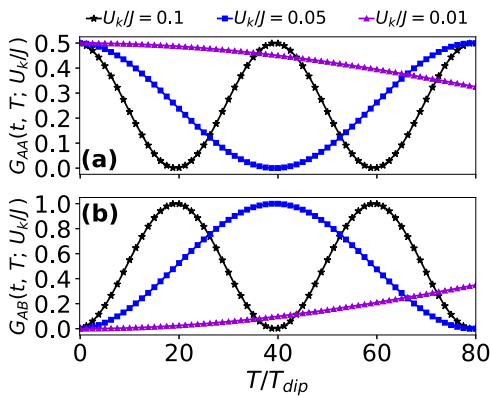


Fig. 8 Output correlations in the analog Ramsey setup at fixed t .

a Behavior of the auto-correlation $G_{AA}(t, T; U_k/J)$ as a function of T/T_{dip} , for $t/T_{dip} = 0.5$, and for different values of U_k/J . **b** Behavior of the cross-correlation $G_{AB}(t, T; U_k/J)$ as a function of T/T_{dip} , for $t/T_{dip} = 0.5$, and for the different values of U_k/J . In both panels, the different curves correspond to the values of U_k/J specified in the top legend.

by $G_{AA}(t, T; U_k/J)$, is maximized close to the condition $t/T_{dip} = 0.5$. The first maximum is located in all the cases at $T/T_{dip} = 0$, i.e. the condition for which the analog setup reduces to the one characterized in the previous section ($2t = T_{dip}$ and $T = 0$). The following peaks of $G_{AA}(t, T; U_k/J)$ as a function of T/T_{dip} explicitly depend on U_k/J . Due to their complementarity, $G_{AB}(t, T; U_k/J)$ is minimized whenever $G_{AA}(t, T; U_k/J)$ is maximized, as it is evident from Fig. 7(d–f).

In addition, these results suggest that the geometry assumed for the device in Fig. 6 is considerably more sensitive to small values of the ratio U_k/J , if compared to the elementary interferometer with a single hopping region. In order to better clarify this point, let us consider a selection of results plotted in Fig. 8, where we show both $G_{AA}(t, T; U_k/J)$ and $G_{AB}(t, T; U_k/J)$ as a function of T/T_{dip} , at fixed $t/T_{dip} = 0.5$ (i.e., following the vertical dashed lines in Fig. 7). In analogy to the Ramsey interferometer, here significant variations in the degree of correlation between the photons emerging at the output of the device are obtained by changing the ratio T/T_{dip} . The latter essentially coincides with varying the distance $L = x_3 - x_2$ between the two interaction regions for a given choice of the hopping distance (d) and the group velocity of the propagating mode (see, e.g., Supplementary Note 1).

As a possible application of this QPIC device, we propose it can be used to extract information about the value U_k (knowing the value of J), by considering the output correlations obtained with devices having an interaction length equivalent to $t/T_{dip} \approx 0.5$ and different values of T/T_{dip} . Notice that $t = 0.5T_{dip}$ corresponds to an interfering region that is only half of the length for the beamsplitting condition in the linear regime ($U_k = 0$), which occurs for $t = T_{dip}$. The reason for the increased sensitivity to the small nonlinear shift can then be traced back to the same reason giving the high sensitivity to small energy shifts in the conventional Ramsey interferometer, given the formal analogy reported above⁶⁰.

QPICs for quantum computing: the $\sqrt{\text{SWAP}}$ gate. Here we analyze the potential application of the QPICs characterized before in quantum information processing. The starting point of our discussion is the behavior displayed in the limit $U_k \gg J$ by the QPIC discussed in “Single hopping region: nonlinear HOM effect” of this subsection. In such a regime, since the presence of two polaritons in the same waveguide is suppressed due to the strong repulsive nonlinearity, the QPIC would implement a

$\sqrt{\text{SWAP}}$ quantum gate⁴³. Indeed, when a single rail qubit encoding is assumed (each waveguiding channel is in logic $|0\rangle$ state if no polariton is present, and logic $|1\rangle$ with a single propagating polariton state), it is straightforward to verify that for $t = T_{dip}$, when using $\{|0_k^A, 0_k^B\rangle, |1_k^A, 0_k^B\rangle, |0_k^A, 1_k^B\rangle, |1_k^A, 1_k^B\rangle\}$ as the two-qubit basis set, the QPIC in Fig. 3 is described by the following matrix operation

$$\sqrt{\text{SWAP}} = \begin{pmatrix} 1 & 0 & 0 & 0 \\ 0 & \frac{1}{\sqrt{2}} & \frac{-i}{\sqrt{2}} & 0 \\ 0 & \frac{-i}{\sqrt{2}} & \frac{1}{\sqrt{2}} & 0 \\ 0 & 0 & 0 & 1 \end{pmatrix}, \quad (27)$$

which allows to implement universal quantum computing when combined with arbitrary single qubit rotations⁴⁴.

However, in order to observe such a behavior one would require a value of U_k that is definitely larger than any nonlinearity expected for polariton systems in conventional material platforms. Hence, the relevant question is: Is there a way to design a device that (i) acts on single polariton states as the nonlinear beam-splitter described in “Single hopping region: nonlinear HOM effect” of this subsection, and also (ii) suppresses polariton bunching in favor of a $G_{AB} = 1$, even in the presence of small U_k/J ? In fact, the simplest device implementing both functionalities is actually the analog Ramsey interferometer characterized before. For what concerns the first operation, it is sufficient to consider the unitary operator defined in Eq. (24) to realize that such a QPIC behaves like a (non-linear) beam-splitter when fed with single-polariton states. Then, regarding the (more challenging) two-qubit operation, it is sufficient to analyse the results of Fig. 8: depending on the value of U_k , there always exists some value for the ratio T/T_{dip} for which $G_{AA} = 0$ and $G_{AB} = 1$. In particular, it can be recognized that such values are roughly determined as $t = T_{dip}/2$ and $T/T_{dip} \approx 2J/U_k$ when $U_k/J \ll 1$. This is obtained by performing a series expansion of Eq. (25) in terms of U_k/J , which after little algebra yields

$$G_{AA}(t, T; U_k/J) \approx \frac{1}{2} \cos^2 \left(\frac{\pi U_k T}{4 J T_{dip}} \right), \quad (28)$$

and

$$G_{AB}(t, T; U_k/J) \approx \sin^2 \left(\frac{\pi U_k T}{4 J T_{dip}} \right). \quad (29)$$

Let us stress the advantages of the proposed scheme: no post-selection is required to implement the quantum gate, and no errors due to state occupancy beyond the computational basis are expected to occur after proper initialization of the system. Thus, the present result holds great promise to realize prospective devices for photonic quantum computing with deterministic gates. In the next section we are going to discuss the effects of inevitable losses in a realistic implementation of this device with propagating polaritons, showing that it is actually feasible in state-of-the-art technology.

Discussion

Here we assess the relevance of the previous theoretical analysis in view of potential applications and realistic experiments in quantum polaritonics. As already mentioned in the “Introduction” section, the polariton-polariton interaction energy has proven to be a quantity that is hard to be probed directly in experiment, although a few reliable estimates exist in the literature^{26,27}. Moreover, such nonlinearities have been shown to be strongly enhanced in suitably engineered nanostructures and exploiting the application of an external electric field⁴⁰, although

the precise enhancement has later been reduced⁴¹. Following recent estimates, we assume a polariton nonlinear interaction energy as large as $U = 15 \mu\text{eV}$ in standard III-V semiconductor technology²⁷, when the polariton field is confined in a spot on the order of $1 \mu\text{m}^2$. In a propagating geometry, even if a polariton wave packet is somehow delocalized in space, this value might be assumed of the same order of magnitude if the wave form spreads by about a wavelength along the propagation direction. In addition, this value might be further enhanced by a factor of 5–10 due to electric field tuning, depending on the different systems reported in the literature^{40,41}, or even exploiting different mechanisms based, e.g., on coupling to the biexciton state⁶¹.

In this section we provide some estimates on the values of U_k that can be detected by a QPIC in realistic scenarios. First, we consider an experimental setup with a single interaction region. A similar device has been experimentally realized¹². The QPIC model based on these system parameters is reported in SI, see Supplementary Note 1. An alternative realization would require working with totally internally reflected propagating polaritons, such as the ones obtained in a planar waveguide⁶², or through a partially etched planar waveguide⁴¹. We notice that the main considerations reported here would not change. In ref. 12 the tunneling rate between two coupled waveguides has been studied as a function of the spatial separation d . A realistic estimate for the tunneling energy, J , is measured to be on the order of $J = 0.5 \text{ meV}$. Hence, the relevant ratio U_k/J would range from 10^{-2} to 10^{-1} in state-of-art devices. These values appear too small to provide a significant deviation from the device operated in a linear regime, as shown in Figs. 4 and 5. On the other hand, such values could be easily detected from correlation measurements in the analog Ramsey setup of Fig. 6, according to the results reported in Figs. 7 and 8, by increasing T . Practically speaking, due to the relation reported in Eq. (26), in order to extrapolate information about the polariton-polariton interaction energy, U_k , it is sufficient to consider the behavior of the cross-correlation function, i.e., double-click events obtained at the output of devices having free propagation region of different lengths L . By collecting data obtained on increasing L (to which T is linearly related through the polariton group velocity, v_g), the double-click statistics would reproduce an oscillating behavior compatible with those reported in Fig. 8(b). Finally, by means of Eqs. (25) and (26), a best fit estimate for the nonlinearity U_k could be straightforwardly extracted.

A further point of discussion is related to the finite polariton lifetime, for which the probability of observing photons emerging from the output channel of the QPIC will necessarily decay on increasing L . The problem of losses has been addressed in detail in Supplementary Note 3, where the finite lifetime of polaritons is treated by means of a Lindblad master equation. On the one hand, as expected, numerical results reveal that the inclusion of a decay rate Γ in the system evolution, such that $\tau = \hbar/\Gamma$, leads to an exponential decay of either populations or correlations with the time spent in the QPIC (i.e., the total length of the device). On the other hand, once correlation functions are properly normalized, i.e.,

$$G_{\alpha\beta} \rightarrow g_{\alpha\beta} = \frac{G_{\alpha\beta}}{\langle \hat{n}_k^\alpha \rangle \langle \hat{n}_k^\beta \rangle} \quad \alpha, \beta = A, B \quad (30)$$

it is found that the behavior in the presence of losses exactly reproduces the one expected for the lossless case. In particular, by considering realistic values for the model parameters¹², such as $J = 0.5 \text{ meV}$ (corresponding to $T_{dip} = \hbar\pi/(4J) \approx 1 \text{ ps}$), polariton decay rate $\Gamma = 0.01 \text{ meV}$ (which corresponds to $\tau \approx 66 \text{ ps}$), and a group velocity in the range from 4 to $5 \mu\text{m}/\text{ps}$, (see also Supplementary Note 1), the range $T/T_{dip} \in [0, 65]$ could be explored

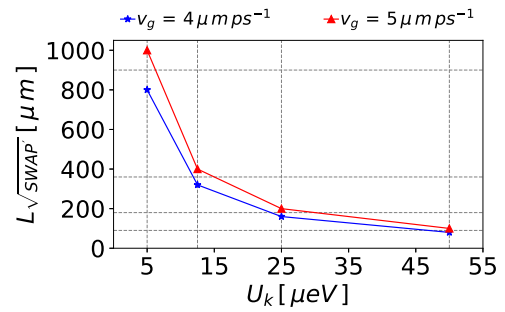


Fig. 9 Ramsey interferometer implementing a $\sqrt{\text{SWAP}}$ gate. Behavior of the free propagation length $L_{\sqrt{\text{SWAP}}} [\mu\text{m}]$ as a function of the nonlinearity $U_k [\mu\text{eV}]$, for two different values of the group velocity v_g . The dashed horizontal and vertical lines have been added as a guide to the eye.

by means of devices having a total length $L_{tot} = v_g(T_{dip} + T)$ of at most $330 \mu\text{m}$. In particular, for such a device length a population decay by at most a $1/e$ factor may be expected in each waveguide. Depending on the value of the ratio U_k/J , such a range of parameters would be large enough to observe (more than) a complete oscillation of the cross-correlations (i.e., for $U_k/J = 0.1$, corresponding to $50 \mu\text{eV}$), or to explore the range $g_{AB} \in [0, 0.25]$ in correspondence of a nonlinearity $U_k = 5 \mu\text{eV}$.

Finally, concerning the specific application of the Ramsey-like interferometric configuration to realize a SWAP-type quantum gate, we explicitly report some realistic device parameters in Fig. 9. In particular, we address the dependence of the free propagation region length for the specific operation in Eq. (27), defined as $L_{\sqrt{\text{SWAP}}}$, as a function of U_k , for some values in the supposedly realistic range $5\text{--}50 \mu\text{eV}$. This length is the L_{tot} corresponding to the condition for which $G_{AA} = 0.0$ (or $G_{AB} = 1.0$, see Fig. 8). Similarly to the previous discussion, we consider two values for the group velocity (as explicitly given in the Figure). A device with a total length $L_{tot} \sim 330 \mu\text{m}$ would be sufficient to implement a full $\sqrt{\text{SWAP}}$ gate, in the presence of a nonlinearity $U_k \approx 15 \mu\text{eV}$, which can be realistically expected on the basis of experimental results reported in the literature. This propagation length is fully within the polariton lifetime of $\tau \sim 66 \text{ ps}$ assumed before. Furthermore, longer lived polaritons might be obtained by using polariton waveguides⁴¹, thus allowing to realize an experimental proof-principle demonstration of this quantum gate even in the presence of smaller nonlinearities. In particular, putting together the effects of losses on the measured coincidences, the following count rates can be expected in realistic experimental scenarios. Measured coincidence rates in the order of $C_R \sim 1 \text{ MHz}$ can be considered for state-of-art single photon sources based on quantum dots, including both demultiplexing and detection efficiencies³⁰. Thus, by assuming in- and out-coupling efficiency to and from the QPIC in the order of $\eta_{in-out} \sim 0.3$ per channel (which is within reach by using state-of-art grating or edge couplers to the polariton chip), and considering a population decay by a $1/e$ factor in each of the two arms, an estimated number of coincidence counts rate can be given as $(\eta_{in}\eta_{out}/e)^2 C_R \approx 1 \text{ kHz}$. This is a very promising result considering that coincidence rates in the order of 1 Hz or lower can nowadays be measured in quantum integrated photonics experiments³⁰.

We conclude this section by discussing the state preparation considered in this work. In our theoretical framework, we assumed the initial two-particles states to correspond to (i) identical and simultaneous polaritons, which (ii) propagate within the QPICs with the same dynamical properties, namely the same wavevector and group velocity. Deviations from these

assumptions may result in non-ideal visibility of the correlation signals measured at the detectors. As already observed in “Model and Theory” subsection of the “Results” section, single quantum emitters can be considered to a large extent as near-optimal single photon sources of indistinguishable quanta^{49,50}. Simultaneous or delayed arrival of these single photon states at the two input ports can be controlled by external means to a large extent. As a consequence, we do believe that the creation of the radiation states needed as input stages for testing the dynamics in QPICs is possible by means of the state-of-the-art technology. Regarding the second issue, since the coupling to the external sources is usually achieved by means of grating couplers, we do observe that only pre-determined wavevectors will enter into the propagation channels. In particular, since the realization of waveguides is subject to lithography and etching processes, it can be controlled to sub-nm precision. This implies that QPICs can be fabricated with almost ideal symmetric single-mode devices.

Conclusion

We have introduced a quantum technology platform that extends current performances of photonic integrated circuits, by exploiting effective interactions between polaritons. We have shown that they allow to build nonlinear quantum devices and deterministic quantum logic gates. As a first step, we have analyzed how polariton interactions can induce a significant deviation from the typical Hong-Ou-Mandel behavior in an integrated beam splitter. Starting from this result, we explicitly designed an integrated polariton interferometer that allows to straightforwardly implement a deterministic $\sqrt{\text{SWAP}}$ gate. By considering realistic experimental conditions and parameters, the proposed QPIC represents a viable route for prospective photonic-based quantum information processing.

Noticeably, the interferometric nature of QPICs makes these devices very well suited also for metrology and sensing purposes. As a targeted example, we have shown how an analog integrated Ramsey interferometer could be used for measuring polariton interaction energies at two-particle level. We thus believe these results will motivate the realization of complex polariton interferometers, which will set the basis of future experiments exploiting the relatively strong nonlinearities of these systems for metrology applications, sensing, quantum simulations, and quantum information processing.

Methods

Numerical simulations for this work have been performed by home made Python codes solving for either the time evolution of the Schrodinger equation or the density matrix master equation.

Data availability

All the data employed for this work will be made available from the authors upon reasonable request.

Code availability

All the codes employed for this work will be made available from the authors upon reasonable request.

Received: 13 July 2021; Accepted: 21 December 2021;

Published online: 03 February 2022

References

- Kasprzak, J. et al. Bose-Einstein condensation of exciton polaritons. *Nature* **443**, 409–414 (2006).
- Balili, R., Hartwell, V., Snoke, D., Pfeiffer, L. & West, K. Bose-Einstein condensation of microcavity polaritons in a trap. *Science* **316**, 1007–1010 (2007).
- Amo, A. et al. Superfluidity of polaritons in semiconductor microcavities. *Nat. Phys.* **5**, 805–810 (2009).
- Amo, A. et al. Polariton superfluids reveal quantum hydrodynamic solitons. *Science* **332**, 1167–1170 (2011).
- Lagoudakis, K. G. et al. Quantized vortices in an exciton-polariton condensate. *Nat. Phys.* **4**, 706–710 (2008).
- Abbarchi, M. et al. Macroscopic quantum self-trapping and josephson oscillations of exciton polaritons. *Nat. Phys.* **9**, 275–279 (2013).
- Nguyen, H. S. et al. Acoustic black hole in a stationary hydrodynamic flow of microcavity polaritons. *Phys. Rev. Lett.* **114**, 036402 (2015).
- Ballarini, D. et al. All-optical polariton transistor. *Nat. Commun.* **4**, 1778 (2013).
- Nguyen, H. S. et al. Realization of a double-barrier resonant tunneling diode for cavity polaritons. *Phys. Rev. Lett.* **110**, 236601 (2013).
- Sturm, C. et al. All-optical phase modulation in a cavity-polariton mach-zehnder interferometer. *Nat. Commun.* **5**, 3278 (2014).
- Marsault, F. et al. Realization of an all optical exciton-polariton router. *Appl. Phys. Lett.* **107**, 201115 (2015).
- Beierlein, J. et al. Propagative oscillations in codirectional polariton waveguide couplers. *Phys. Rev. Lett.* **126**, 075302 (2021).
- Azzini, S. et al. Ultra-low threshold polariton lasing in photonic crystal cavities. *Appl. Phys. Lett.* **99**, 111106 (2011).
- Liew, T. C. H. et al. Exciton-polariton integrated circuits. *Phys. Rev. B* **82**, 033302 (2010).
- Liew, T. C. H., Kavokin, A. V. & Shelykh, I. A. Optical circuits based on polariton neurons in semiconductor microcavities. *Phys. Rev. Lett.* **101**, 016402 (2008).
- Andreani, L. C. & Pasquarello, A. Accurate theory of excitons in GaAs-Ga_{1-x}Al_xAs quantum wells. *Phys. Rev. B* **42**, 8928–8938 (1990).
- Kavokin, A., Baumberg, J. J., Malpuech, G. & Laussy, F. P. *Microcavities* (Oxford Science, 2008).
- Sanvitto, D. & Kéna-Cohen, S. The road towards polaritonic devices. *Nature Materials* **15**, 1061–1073 (2016).
- Ciuti, C., Savona, V., Piermarocchi, C., Quattropani, A. & Schwendimann, P. Role of the exchange of carriers in elastic exciton-exciton scattering in quantum wells. *Phys. Rev. B* **58**, 7926–7933 (1998).
- Tassone, F. & Yamamoto, Y. Exciton-exciton scattering dynamics in a semiconductor microcavity and stimulated scattering into polaritons. *Phys. Rev. B* **59**, 10830–10842 (1999).
- Carusotto, I. & Ciuti, C. Quantum fluids of light. *Rev. Mod. Phys.* **85**, 299–366 (2013).
- Ghosh, S. & Liew, T. C. H. Quantum computing with exciton-polariton condensates. *npj Quantum Inf.* **6**, 16 (2020).
- Solnyshkov, D. D., Bleu, O. & Malpuech, G. All optical controlled-not gate based on an exciton-polariton circuit. *Superlattices Microstructures* **83**, 466–475 (2015).
- Cuevas, Á. et al. First observation of the quantized exciton-polariton field and effect of interactions on a single polariton. *Sci. Adv.* **4**, ea06814 (2018).
- Suárez-Forero, D. G. et al. Quantum hydrodynamics of a single particle. *Light.: Sci. Appl.* **9**, 85 (2020).
- Muñoz-Matutano, G. et al. Emergence of quantum correlations from interacting fibre-cavity polaritons. *Nat. Mater.* **18**, 213–218 (2019).
- Deltiel, A. et al. Towards polariton blockade of confined exciton-polaritons. *Nat. Mater.* **18**, 219–222 (2019).
- Brod, D. J. et al. Photonic implementation of boson sampling: a review. *Adv. Photonics* **1**, 034001 (2019).
- Aaronson, S. & Arkhipov, A. The computational complexity of linear optics. In *Proceedings of the Forty-Third Annual ACM Symposium on Theory of Computing*, STOC '11, 333–342 (Association for Computing Machinery, New York, NY, USA, 2011). <https://doi.org/10.1145/1993636.1993682>
- Wang, H. et al. Boson sampling with 20 input photons and a 60-mode interferometer in a 10¹⁴-dimensional hilbert space. *Phys. Rev. Lett.* **123**, 250503 (2019).
- Zhong, H.-S. et al. Quantum computational advantage using photons. *Science* **370**, 1460–1463 (2020).
- Spagnolo, N., Brod, D. J., Galvao, E. F. & Sciarrino, F. Non-linear boson sampling. *arxiv2110.13788* (2021).
- Knill, E., Laflamme, R. & Milburn, G. J. A scheme for efficient quantum computation with linear optics. *Nature* **409**, 46–52 (2001).
- Ralph, T. C., Langford, N. K., Bell, T. B. & White, A. G. Linear optical controlled-not gate in the coincidence basis. *Phys. Rev. A* **65**, 062324 (2002).
- Calafell, I. A. et al. Quantum computing with graphene plasmons. *npj Quantum Inf.* **5**, 37 (2019).
- Heuck, M., Jacobs, K. & Englund, D. R. Controlled-phase gate using dynamically coupled cavities and optical nonlinearities. *Phys. Rev. Lett.* **124**, 160501 (2020).
- Li, M. et al. Photon-photon quantum phase gate in a photonic molecule with $\chi^{(2)}$ nonlinearity. *Phys. Rev. Appl.* **13**, 044013 (2020).
- Preskill, J. Quantum Computing in the NISQ era and beyond. *Quantum* **2**, 79 (2018).

39. Ferrier, L. et al. Interactions in confined polariton condensates. *Phys. Rev. Lett.* **106**, 126401 (2011).
40. Rosenberg, I. et al. Strongly interacting dipolar-polaritons. *Sci. Adv.* **4**, eaat8880 (2018).
41. Suárez-Forero, D. G. et al. Enhancement of parametric effects in polariton waveguides induced by dipolar interactions. *Phys. Rev. Lett.* **126**, 137401 (2021).
42. López Carreño, J., Sánchez Muñoz, C., Sanvitto, D., del Valle, E. & Laussy, F. Exciting polaritons with quantum light. *Phys. Rev. Lett.* **115**, 196402 (2015).
43. Franson, J. D., Jacobs, B. C. & Pittman, T. B. Quantum computing using single photons and the zeno effect. *Phys. Rev. A* **70**, 062302 (2004).
44. Nielsen, M. A. & Chuang, I. L. Quantum computation and quantum information (Cambridge University Press, Cambridge, UK, 2010).
45. Politi, A., Cryan, M. J., Rarity, J. G., Yu, S. & O'Brien, J. L. Silica-on-silicon waveguide quantum circuits. *Science* **320**, 646–649 (2008).
46. Crespi, A. et al. Integrated multimode interferometers with arbitrary designs for photonic boson sampling. *Nat. Photonics* **7**, 545–549 (2013).
47. Metcalf, B. J. et al. Multiphoton quantum interference in a multiport integrated photonic device. *Nat. Commun.* **4**, 1356 (2013).
48. Nelsen, B. et al. Dissipationless flow and sharp threshold of a polariton condensate with long lifetime. *Phys. Rev. X* **3**, 041015 (2013).
49. Loredò, J. C. et al. Boson sampling with single-photon fock states from a bright solid-state source. *Phys. Rev. Lett.* **118**, 130503 (2017).
50. Somaschi, N. et al. Near-optimal single-photon sources in the solid state. *Nat. Photonics* **10**, 340–345 (2016).
51. Hong, C. K., Ou, Z. Y. & Mandel, L. Measurement of subpicosecond time intervals between two photons by interference. *Phys. Rev. Lett.* **59**, 2044–2046 (1987).
52. Heeres, R. W., Kouwenhoven, L. P. & Zwiller, V. Quantum interference in plasmonic circuits. *Nat. Nanotechnol.* **8**, 719–722 (2013).
53. Spagnolo, N. et al. General rules for bosonic bunching in multimode interferometers. *Phys. Rev. Lett.* **111**, 130503 (2013).
54. Luo, K.-H. et al. Nonlinear integrated quantum electro-optic circuits. *Sci. Adv.* **5**, eaat1451 (2019).
55. Pittman, T. B. et al. Can two-photon interference be considered the interference of two photons? *Phys. Rev. Lett.* **77**, 1917–1920 (1996).
56. Verger, A., Ciuti, C. & Carusotto, I. Polariton quantum blockade in a photonic dot. *Phys. Rev. B* **73**, 193306 (2006).
57. Gerace, D., Laussy, F. & Sanvitto, D. Quantum nonlinearities at the single-particle level. *Nat. Mater.* **18**, 200–201 (2019).
58. Carusotto, I. et al. Fermionized photons in an array of driven dissipative nonlinear cavities. *Phys. Rev. Lett.* **103**, 033601 (2009).
59. Gerace, D., Türeci, H. E., Imamoglu, A., Giovannetti, V. & Fazio, R. The quantum-optical josephson interferometer. *Nat. Phys.* **5**, 281–284 (2009).
60. Cohen-Tannoudji, C. & Guéry-Odelin, D. Advances in atomic physics (World Scientific, 2011).
61. Carusotto, I., Volz, T. & Imamoglu, A. Feshbach blockade: Single-photon nonlinear optics using resonantly enhanced cavity polariton scattering from biexciton states. *EPL (Europhys. Lett.)* **90**, 37001 (2010).
62. Walker, P. M. et al. Exciton polaritons in semiconductor waveguides. *Appl. Phys. Lett.* **102**, 012109 (2013).

Acknowledgements

We acknowledge financial support from the Italian Ministry of Research (MIUR) through the PRIN 2017 project “Interacting photons in polariton circuits” (INPhoPOL). Useful discussions with V. Ardizzone, D. Ballarini, A. Gianfrate, E. Maggolini, D. Suárez-Forero are gratefully acknowledged.

Author contributions

D.N. proposed the original idea of the analog Ramsey interferometer for polaritons, and performed all the numerical simulations. D.G. supervised the work; D.N., V.D'A., D.S., and D.G. discussed the results, their interpretation, and the physical realization of the proposed devices. D.N. and D.G. drafted the first version of the manuscript, with key inputs from all the authors to produce the final version.

Competing interests

The authors declare no competing interests.

Additional information

Supplementary information The online version contains supplementary material available at <https://doi.org/10.1038/s42005-022-00810-9>.

Correspondence and requests for materials should be addressed to Davide Nigro or Dario Gerace.

Peer review information *Communications Physics* thanks the anonymous reviewers for their contribution to the peer review of this work. Peer reviewer reports are available.

Reprints and permission information is available at <http://www.nature.com/reprints>

Publisher's note Springer Nature remains neutral with regard to jurisdictional claims in published maps and institutional affiliations.



Open Access This article is licensed under a Creative Commons Attribution 4.0 International License, which permits use, sharing, adaptation, distribution and reproduction in any medium or format, as long as you give appropriate credit to the original author(s) and the source, provide a link to the Creative Commons license, and indicate if changes were made. The images or other third party material in this article are included in the article's Creative Commons license, unless indicated otherwise in a credit line to the material. If material is not included in the article's Creative Commons license and your intended use is not permitted by statutory regulation or exceeds the permitted use, you will need to obtain permission directly from the copyright holder. To view a copy of this license, visit <http://creativecommons.org/licenses/by/4.0/>.

© The Author(s) 2022